**Structure-activity relationships of Au/ZrO<inf>2</inf> catalysts for 5-hydroxymethylfurfural oxidative esterification: Effects of zirconia sulphation on gold dispersion, position and shape**

**Structure-activity relationships of $Au/ZrO_2$ catalysts for 5-hydroxymethylfurfural oxidative esterification: effects of zirconia sulphation on gold dispersion, position and shape**

Federica Menegazzo[a], Michela Signoretto[a*], Damiano Marchese[a], Francesco Pinna[a], Maela Manzoli[b]

[a]*Department of Molecular Sciences and Nanosystems, Ca' Foscari University Venice and INSTM-RU Ve, Dorsoduro 2137, 30123 Venezia (Italy)*

[b]*Department of Chemistry & NIS Interdepartmental Centre, University of Turin, Via P. Giuria 7, 10125 Turin, Italy*

*Corresponding author:
Prof. Michela Signoretto,
miky@unive.it
phone number: +39 041-2348650

**Key words:** gold catalyst; sulphated zirconia; HMF, oxidation; esterification; biomass; FDCA; FDMC; deposition-precipitation; irregular plate-like gold nanoparticles.

**Abstract**

The oxidative esterification of 5-hydroxymethylfurfural (HMF) to furan-2,5-dimethylcarboxylate (FDMC) has been investigated on $Au/ZrO_2$ catalysts. We have examined bare zirconia and sulphated zirconia with different amounts of sulphates in order to identify the effects of the sulphation pretreatment. The amount of sulphate groups present on zirconia regulates the gold amount and dispersion, as well as its shape and position. It has been found that the reactivity is associated not only to the Au active phase, in terms of loading and size, but it is also closely tied to its shape and distribution on the support. Irregular plate-like gold nanoparticles have been observed on the sulphated samples and they affect the selectivity to FDMC. Structure-properties relationships have been determined and a model has been proposed.

## Introduction

The catalytic conversion of biomasses provides a sustainable alternative to produce non-fossil-based chemicals and biofuels. Such opportunity can reduce the dependence from petroleum-based resources [1]. Actually, carbohydrates coming from biomass can be considered the most abundant renewable resource [2]. The nonedible nature of lignocellulose, which implies no competition with food, makes this an important raw material for biorefineries in the future. According to Scheme 1, lignocellulosic biomass is a complex matrix of cellulose, hemicellulose and lignin. It contains two types of sugars: hexoses and pentoses, the "C6" and "C5" fractions, respectively.

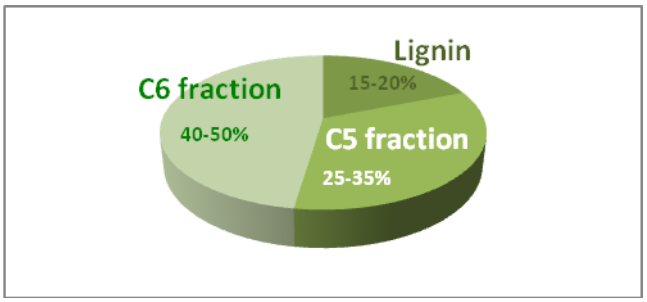


**Scheme 1**. Composition of lignocellulosic biomass.

The transformation of selected platform molecules is the most appropriate approach for identifying molecules that can replace those coming from petrolchemistry or for the generation of new molecules that display improved or different properties. The transformation of 5-hydroxymethylfurfural (HMF) in valuable furan derivates for biofuel and fine chemical industry is an example of this approach [3, 4]. HMF can be produced by acid-catalyzed dehydration of lignocellulosic building blocks such as glucose and fructose, as well as directly from cellulose [5].

HMF is a versatile intermediate that can be further transformed into a wide variety of high performance and high value-added chemicals. Among the various conversion routes, the HMF molecule can be catalytically oxidized to 2,5 furandicarboxylic acid (FDCA). The catalytic oxidation to FDCA is an essential process, because FDCA has been recently proposed as a possible alternative for

terephthalic acid [6] which is the monomer used for the production of polyethylenterephthalate (PET) plastic.

Actually, PET is mainly manufactured through the purified terephthalic acid, whose process is based on the liquid-phase oxidation of p-xylene [7, 8]. Bioaccumulation in living organisms displayed by phthalates and derived polymers have driven towards new alternative routes. The polymer that can be produced starting from FDCA (PEF) presents a lot of advantages: (i) it is obtained from a bio-derived, renewable raw material, (ii) it is more easily degradable and above all, (iii) it does not present bioaccumulation problems. However, FDCA is practically insoluble in most of the solvents industrially used. A promising alternative is the HMF oxidative esterification into the corresponding furan-2,5-dimethylcarboxylate (FDMC), according to Scheme 2.

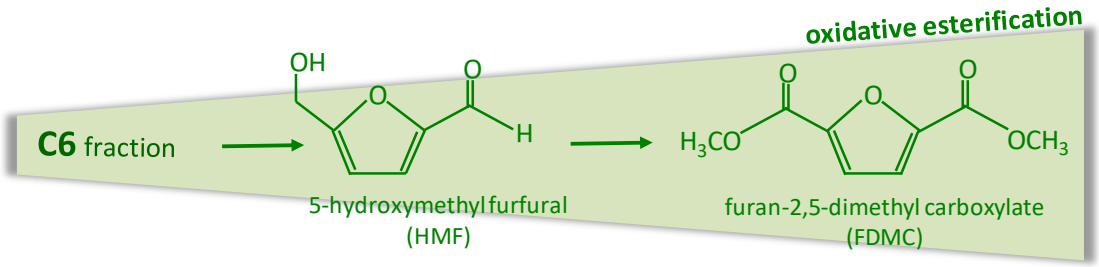


**Scheme 2**. HMF oxidative esterification reaction.

The FDMC molecule can be easily purified by low-temperature sublimation to give high purity FDMC, which is readily soluble in the most common solvents and therefore it could be even more suitable than FDCA as monomer for the replacement of terephtalic acid in plastics [9, 10].

Some reviews on the selective oxidation of furan derivates [11-13] have been published in the last years, meaning that a great attention has been paid to these reactions. The necessity of the clean production of value-added chemicals, such as FDMC from HMF, increased the demand for aerobic catalysts that use molecular oxygen as oxidant and produce only water as byproduct. The use of heterogeneous catalysts would be of particular interest because HMF can be easily oxidized, being an alcohol and an aldehyde at the same time. Recently, gold catalysts have received attention as promising oxidation candidates [9, 10, 14-16], indicating that the choice of gold nanoparticles is advantageous for oxidative esterification reactions.

Good yields in the HMF oxidative esterification were obtained by using the $Au/TiO_2$ reference catalyst provided by the World Gold Council in the presence of a base (8% $CH_3ONa$) [9]. However, the use of the base makes the process less environmentally and economically advantageous. To overcome such problem Corma et al [10] tested this reaction over gold based catalysts on different supports, without using the base. Satisfactory performances were observed only in the case of one particular catalyst dispersed on ceria nanoparticles, while the other samples require reaction times ranging from 24 to 72 hours to get still very low yields.

Very recently, we investigated gold catalysts supported on zirconia [17, 18], ceria and titania [19] for a base-free esterification of furfural. In particular, the comparison among Au samples with similar metal content over different supports revealed that the catalytic performances follow the trend: Au/zirconia > Au/ceria> >Au/titania. The furoate ester can be obtained with optimal yields by taking into account both Au nanosize (for good conversion) and acidity/basicity properties of the support (for good selectivity). The results for HMF oxidative esterification have shown that in reaction conditions, oxygen is fundamental to keep the active surface sites free, in particular the highly dispersed gold sites, where oxygen can be dissociated [20]. As a consequence, the dispersion of gold is a crucial point, due to the role played by basic oxygen atoms in the activation of both methanol and HMF reactants.

In the past years, we have demonstrated that sulphates act as structural promoters of the zirconia support. In particular, the addition of sulphates plays a positive role, resulting in an enhancement of the surface area of the oxide and in a higher gold dispersion [21]. However, no sulphates are present in the final catalysts anymore, due to the detachment of sulphate groups during the deposition-precipitation at pH=8.6.

In the present paper, we investigated the role of the sulphation degree of zirconia on the nature and dispersion of supported gold species and consequently on the catalytic properties. In particular, such a screening on sulphation has been carried out in order to further improve catalytic performances of the $Au/ZrO_2$ system for the HMF oxidative esterification reaction in the absence of $NaCH_3O$. Au/zirconia catalysts with the same gold loading and in which with different amount of sulphates have been added before the metal introduction will be examined. The results will be compared with those

obtained from a gold catalyst supported on plain zirconia and one reference catalyst provided by the World Gold Council.

## 2. Experimental

*Catalyst preparation*

$Zr(OH)_4$ was prepared by precipitation with ammonia (5M) from $ZrOCl_2 \cdot 8H_2O$ at constant pH= 8.6, aged for 20 hours at 90 °C and then dried at 110 °C for 20 hours. Part of the hydroxide was sulphated with $(NH_4)_2SO_4$ (Merck) by incipient wetness impregnation in order to obtain a 2 or 8 wt % amount of sulphates on the final support. Then zirconium hydroxide (Z) and sulphated zirconium hydroxides (SZ2 and SZ8) were calcined in air (30 ml/min STP) at 650 °C for 3 hours.

Gold was added by deposition-precipitation (dp) at pH=8.6 in order to obtain a nominal 1.5 wt% Au. An aqueous solution of $HAuCl_4 \cdot 3H_2O$ was lead to pH=8.6 by the addition of NaOH (0,5 M). The oxides were quickly added and the pH was controlled by the addition of NaOH (0,5 M). After 3 hours the samples were filtered, washed twice with distilled water and dried at 35 °C overnight. Finally samples were calcined in air for 1 hour at 400 °C in order to create a stronger interaction between the metal and the support, and therefore to stabilize the gold active sites. The obtained samples will be hereafter denoted as AuZ, AuSZ2 and AuSZ8, respectively.

In addition, $Au/TiO_2$ provided by the WGC was used as reference catalyst (AuWGC). [22].

*Methods*

Surface areas and pore size distributions were obtained from $N_2$ adsorption/desorption isotherms at -196 °C (using a Micromeritics ASAP 2000 analyser). Surface areas were calculated from the $N_2$ adsorption isotherms by the BET equation, and pore size distribution were determined by the BJH method [23]. Total pore volumes were taken at $p/p_0 = 0.99$.

The sulphate content was determined by ion chromatography (IC). Sulphate concentration was calculated as the average of two independent analyses, each including two chromatographic determinations.

The gold amount was determined by atomic adsorption spectroscopy after microwave destruction of the samples (100 mg).

X-ray powder diffraction (XRD) patterns were measured by a Bruker D8 Advance diffractometer equipped with a Si(Li) solid state detector (SOL-X) and a sealed tube providing Cu $K_\alpha$ radiation.

CO pulse chemisorption measurements were performed at -116 °C in a lab-made equipment.

CO adsorption on the Au catalysts has been investigated also by means of transmission FTIR measurements, performed on the samples in self-supporting pellets introduced in a cell allowing thermal treatments in controlled atmospheres and spectrum scanning at controlled temperatures (from -196 °C to 25 °C). The FTIR spectra were taken on a Bruker IFS 66 spectrometer (equipped with a cryogenic MCT detector). The spectra were normalised respect to the weight of the pellet and to the effective gold content reported in Table 2.

For diffuse reflectance UV–Vis-NIR analysis, powders were placed in a quartz cell, allowing treatments in controlled atmosphere and temperature, but spectra recording only at room temperature (r.t.). Diffuse reflectance UV–Vis-NIR spectra were run at r.t. on a Varian Cary 5000 spectrophotometer, working in the range of wavenumbers 190-2500 nm. UV–Vis-NIR spectra are reported in the Kubelka-Munk function [$f(R\infty)=(1-R\infty)2/2R\infty$; $R\infty$=reflectance of an "infinitely thick" layer of the sample.

Electron micrographs were obtained by a Jeol 3010-UHR high resolution transmission electron microscope (HRTEM) operating at 300 kV equipped with a $LaB_6$ filament and with an Oxford Inca Energy TEM 300 EDS X-rays analyzer by Oxford Link. Digital micrographs were acquired by an Ultrascan 1000 camera and processed by Gatan digital micrograph.

*Catalytic activity measurement*

HMF oxidative esterification reactions were investigated without $NaCH_3O$ addition, using a mechanical stirred autoclave fitted with an external jacket [18]. Catalyst (100 mg), substrate (200 mg of 5-hydroxymethylfurfural, Sigma Aldrich 99%) and n-octane (150 μl), used as internal standard, were added to methanol (150 ml). The methanol behaves both as a solvent and as a reagent for the oxidative esterification. The

reactor was charged with the oxygen (3 bar), stirred at 1000 rpm and heated at 130 °C. The progress of the reaction was determined after 5 hours by gas-chromatographic analysis of the converted mixture (capillary column HP-5, FID detector). Preliminary experiments showed that the system works in a strictly kinetic regime [18].

## 3. Results and Discussion

### *3.1. Preliminary characterization of the supports*

Very recently, we compared Au samples with similar metal content over different supports for the oxidative esterification of furfural [19]. The Au/zirconia system displayed the best catalytic performances indicating that the chemical and morphological properties observed for the zirconia-based catalyst seem to fulfill a compromise between high gold dispersion and the need of non acid or basic sites exposed by the support. It is well known that the sulphation procedure induces an increase of the surface area of zirconia as well as a decrease of the mean pore size. Moreover, we have already demonstrated [21] additional advantages for a $Au/ZrO_2$ system when sulphates are added to the zirconia support: i) higher gold dispersion due to higher surface area; ii) higher gold dispersion due to the positive role of $SO_4^{=}$ groups that address the deposition of Au in the form of highly dispersed gold in close contact with the support. In the present paper, a screening on sulphation has been carried out in order to further improve catalytic performances of the $Au/ZrO_2$ system for the HMF oxidative esterification. The supports prepared and employed are: zirconia (Z), a 2 wt% sulphated zirconia (SZ2) and a 8 wt% sulphated zirconia (SZ8). The textural properties of the three supports are reported in Table 1.

After the calcination of hydroxides, the $SO_4^{=}$ amount of each sample is lower than the nominal content. In particular, the difference between the nominal and the real values increases with increasing the content of effectively present anions. It is known [25] that the elimination of sulphates occurs during the calcination step, and that the $SO_4^{=}$ amount that remains at the end of this process is strictly connected with the calcination conditions. It was observed that about four $SO_4^{=}$ groups/$nm^2$ are present on the zirconia surface after calcination in air at temperature close to that used in this work (650 °C) [26]. Such amount is related to those anions which are firmly anchored to $Zr^{4+}$ sites preferably located on the terraces of the zirconia crystallites. Indeed, $SO_4^{=}$ groups linked

to $Zr^{4+}$ edges and corners are energetically richer if compared to the previous ones and, as a consequence, sulphates associated to edges and corners sites are promptly decomposed during calcination. In other words, there is a sort of selective elimination of sulphates from highly energetic crystallographic defects [26]. The relationship between the loss of sulphates and their final amount is regulated by the maximum amount of anions that the oxide can keep under the calcination conditions. Therefore, we can assume a maximum value of about 4%wt/wt for the samples object of the present work.
The nature of the zirconia phases has been investigated by XRD analyses. The results obtained for the three supports are shown in Figure 1. It can be observed that the ratio tetragonal/monocline phase of zirconia increases with the amount of sulphates. In particular, plain zirconia presents mainly the monocline phase, while SZ8 support clearly shows the preponderance of the tetragonal phase, in agreement with previous findings [21]. Indeed, the presence of sulphates ions on the support favors the stabilization of the metastable tetragonal phase on zirconia during the calcination step. The latter phase has a higher surface area than the monoclinic one. This effect is important because, in principle, a high surface area allows a better dispersion of the active phase on the support, as previously demonstrated [21].
$N_2$ physisorption analyses have been performed to confirm the effect of the presence of $SO_4^{=}$ on the surface area. Figure 2 shows absorption/desorption isotherms for the three zirconia samples. In all cases, type IV isotherms are observed, indicating a mesoporous material, with a H1 type hysteresis, representing systems with homogeneous cylindric channels. By applying the BET model, we obtained the surface areas reported in Table 1. In agreement with literature data, an effect of sulphates addition is evident: an increase in sulphates amount leads to a corresponding increase in surface area (SZ8>SZ2>Z). The presence of sulphates ions on the support is crucial during the calcination step, as sulphate groups are able to stabilize the metastable tetragonal zirconia phase which has a higher surface area than the monoclinic phase. This is in agreement with the previously discussed XRD data. Moreover, the BHJ pore size distributions are all unimodal, as shown in the inset of Figure 2. The support without sulphates presents a narrower pore size distribution and a mean pore size shifted towards higher values than the sulphated supports.

*3.2. Characterization of the catalysts*

Table 2 summarizes the characterization data of the catalysts obtained starting from the supports described in the previous section together with the data concerning the AuWGC sample.

A comparison between Table 1 and Table 2 points out that both surface area and porosity of the supports and of the corresponding catalysts are very similar, proving that they are not modified by the deposition-precipitation of gold during the synthesis.

The actual Au wt% increases with the amount of sulphates: it can be proposed that sulphates facilitate the deposition of the active phase. As expected, no residual sulphates were found by ion chromatography after gold deposition-precipitation at pH=8.6 [21].

Chemisorption analyses were also carried out in order to evaluate the gold dispersion. Looking at the results reported as $mol_{CO}/mol_{Au}$ ratios (Table 2), an effect of the previous sulphates addition on the consequent dispersion of the active phase can be proposed. Despite a quite similar Au content, the AuWGC catalyst displays a lower $mol_{CO}/mol_{Au}$ ratio than the samples examined in this study.

X-ray diffraction measurements were performed to establish the nature of the crystallographic phases of the support and to check the eventual presence of crystalline Au nanoparticles. The comparison among the three samples is reported in Figure 3, section a.

Similarly to what observed in the XRD patterns related to the supports (see Figure 1), the ratio between tetragonal/monocline phases of zirconia increases with the amount of sulphates on the support. XRD confirmed the presence of a very small amount of crystalline gold as demonstrated by the weak peak at $2\theta = 38.2\ °$ (zoom shown in section b of Figure 4). In agreement with the CO chemisorption findings, the intensity of the peak at $2\theta = 38.2\ °$ follows the trend: AuZ >AuSZ2>AuSZ8.

FTIR spectroscopy of adsorbed CO was performed on the zirconia-containing samples and the results are reported in Figure 4. The samples were previously activated and further hydrated to reproduce the same experimental conditions adopted for the chemisorption measurements (see the SI section).

Quite big differences as for the intensity of the band at 2093 $cm^{-1}$, related to linear carbonyls on Au sites [24], are evident for the three samples. The spectra have been normalized on the weight of the pellets and on the effective gold loading. Therefore, the

intensity of the band at 2093 $cm^{-1}$ can be taken as a measure of the abundance of the exposed gold sites on the different samples. On the contrary, this assumption is not valid as for the different intensity of the band observed at 2150 $cm^{-1}$, due to CO in interaction with the OH groups, because in this case normalization on the surface areas of the supports would have been necessary. In agreement with chemisorption and XRD findings, the amount of exposed Au sites follows the trend: AuZS8>AuZS2>AuZ, strengthening a role of sulphates on gold dispersion.

*3.3. Catalytic results*

In Figure 5 the results of the catalytic activity and selectivity of the three gold catalysts together with those related to the reference $Au/TiO_2$ provided by the WGC (AuWGC) catalyst are shown.

It can be observed that the conversion is 100% for all zirconia supported samples, whilst the reference AuWGC sample reaches a conversion of 90%, despite containing 1.5 wt% Au, that is a value comparable to that found for our samples. These results are an indication that the amount of Au exposed sites is not directly correlated to the catalytic activity of the catalysts supported on zirconia and that not all the Au exposed sites are active sites. As for the selectivity, AuWGC shows again the worst performance (6%) if compared to the other catalysts (in the 19-32% range). A bell-shaped trend displayed by the gold-zirconia catalysts is evident. In particular, the maximum selectivity is reached by the AuSZ2 catalyst (32%), while AuSZ8 presents a value of 19%. It can be assumed that there is a range of sulphates concentration in which they have a positive effect and the activity of the catalyst results enhanced. This effect is due neither to the amount of Au nor to the size of the gold nanoparticles, as indicated by the findings discussed previously. Indeed, chemisorption, XRD and FTIR analyses concur in establishing that the amount of exposed Au sites follows the trend: AuSZ8>AuSZ2>AuZ.

The large difference observed in terms of selectivity between AuSZ2 and AuSZ8 could be explained by hypothesizing an effect of sulphates on the gold active sites; a possible mechanism is reported in Scheme 3.

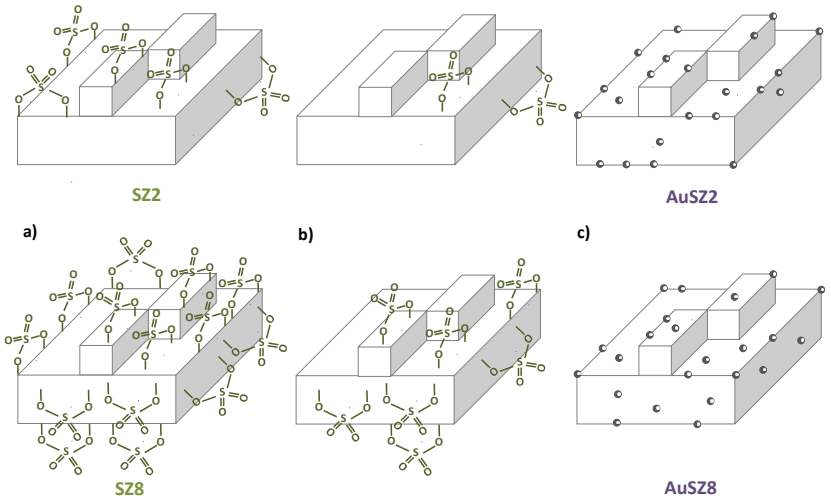


**Scheme 3** Possible mechanism of the effect of sulphates on gold active phase: a) different amounts of sulphated groups on zirconia; b) calcination at 650 °C; c) deposition-precipitation of gold (represented by violet spheres).

The activity of a catalytic system is related firstly to the amount and the dispersion of the active phase, but it is also closely tied to the distribution of the active phase on the support.

The support can be described as a three-dimensional system in which terraces, edges, corners, etc. are present. All these sites possess some deficiencies, and therefore a different reactivity. A fraction of sulphate ions present on the support is removed during calcination. In particular, the more defective sites, being the most reactive, are the first to be vacated and, as a consequence, these sites are available for the attachment of the gold active phase, i.e. the $Au(OH)_3$ precursor. In our case, the sulphate groups present on the edges, on the corners and in general on the defective sites are firstly eliminated from the SZ2 support during the calcination step (upper part of Scheme 3, sections a and b). Therefore, the active phase will be preferentially localized on these sites after gold deposition-precipitation (section c). On the contrary, in the case of the SZ8 support, where an higher amount of sulphates is present (lower part of scheme 3, section a) a large fraction of them persist on the corners and edges as well as on the less defective terraces even after calcination (section b). The presence of residual sulphates is able to influence the subsequent deposition-precipitation phase. Indeed, the edged and the corners will not be available for the $Au(OH)_3$ precursor during deposition-

precipitation and therefore a large fraction of the gold nanoparticles will be presumably localized on the terraces of zirconia, too.

In order to confirm our hypothesis on the mechanism of the effects of sulphates amount and to further elucidate the catalytic results additional analyses have been carried out.

### *3.4. Effect of sulphation degree of zirconia on the nature and reactivity of supported gold species*

Diffuse reflectance UV-Vis-NIR measurements were undertaken with the aim to get further information on the nature of the Au phase, the spectra of the as prepared samples are reported in Figure 6 in the 400-800 nm region, in order to focus on the plasmonic absorption of gold.

The catalysts showed different colors, violet, purple and grey, and different color intensities as can be seen in Figure 7.

Thus, in all cases, a broad absorption in the wavelength range of 500-650 nm, corresponding to the observed colors of powders, has been observed. The zirconia support, either bare or sulphated, is a white powder and the related UV-Vis spectra do not show any band in the above region (data not shown for the sake of brevity). Therefore, the observed absorption can be assigned to the localized surface plasmon resonance (LSPR) of supported gold [27], confirming the presence of Au nanoparticles. However, looking at the spectra, it can be observed that the maxima have different position and shape, as summarized in Table 3.

In particular, AuWGC shows the most intense plasmonic absorption at 545 nm, whereas the UV-Vis spectrum related to AuZ displays a blue shifted maximum, indicating a higher metal dispersion than AuWGC, in agreement with the previous findings. Both LSPR absorptions of AuSZ2 and AuSZ8 have a broader shape. A deconvolution procedure put in evidence that these maxima are the results of the presence of two superimposed components, the former blue shifted in position if compared to the previous two samples, indicating the presence of smaller nanoparticles [28-30], whilst the latter is in a red shifted position. The presence of a component at higher wavelengths cannot be explained by assuming the presence of gold particles with greater size, because it would be in sharp contrast with the previous characterization results. Indeed, the AuZ catalyst, which is the one with the lowest dispersion, the weakest band of

adsorbed CO and the highest intensity of the peak related to crystalline gold, does not show such absorption. Nevertheless, the red shifted component is clearly related to the sulphation procedure, being more pronounced by increasing the sulphates amount. It can be proposed that, besides guaranteeing a higher dispersion of gold, the presence of sulphates could address the metal to specific shapes.

A careful HRTEM analysis has been carried out on the AuSZ8 sample and the results are summarized in Figure 8. Roundish gold nanoparticles (section a) as well as irregular plate-like nanoparticles with diameter above 3 nm (section b) have been observed. The particle size distribution indicates that the majority of the gold species has size between 2 and 3 nm, being the average size equal to 2.5 nm (section c).

Due to the intrinsic complexity, the impact of the nanoparticles shape on the LSPR has been far less studied. However, a variety of gold shapes such as disks [31], triangular, square and hexagonal shapes, as well as cube-shaped particles has been synthesized [32]. It has been reported that the plasmonic properties of gold nanostructures can be engineered for different applications [33]. E. Kowalska et al. explained the photocatalytic activity of different $Au/TiO_2$ catalysts in terms of light absorption ability in a wide wavelength range resulting from transverse and longitudinal LSPR of rod-like gold particles [27]. It has already reported that rod-like shapes exhibit both transverse and longitudinal plasmons at 520-530 nm and 600 nm [34, 35]. "Branched" gold nanocrystals exhibit a shape-dependent plasmon resonance that is red-shifted by 130-180 nm from the spherical particle wavelength [36].

It can be suggested that the irregular plate-like gold nanoparticles observed on the AuSZ8 sample are responsible for the plasmonic contribution at high wavelenghts. Moreover, AuSZ8 show a more pronounced red shift of the component at high wavelengths if compared to AuSZ2, indicating the presence of different amounts of plate-like gold nanoparticles, according to Scheme 4.

It can be proposed that on SZ8 support the gold precursor does not find edges and corners available during deposition-precipitation and most of the gold species will be localized on the terrace sites of zirconia, agglomerating into irregular plate-like nanoparticles. Such shape of gold nanoparticles is responsible for the drop in selectivity.

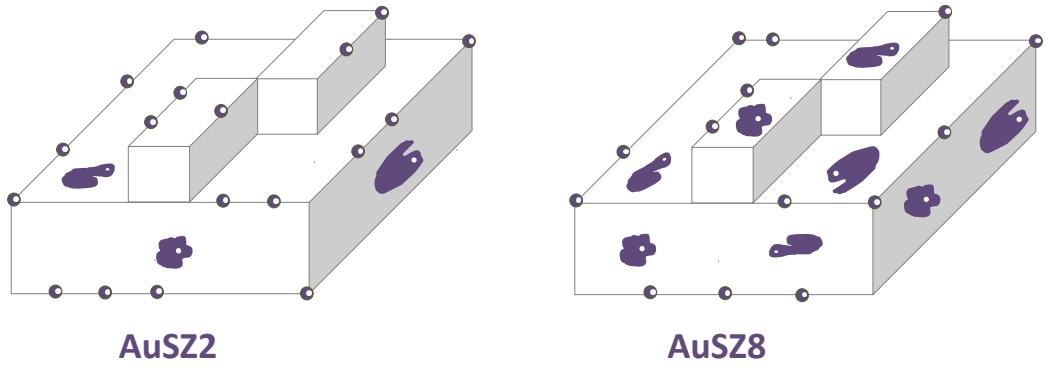


**Scheme 4:** Possible effect of sulphates on the shape of gold species: deposition-precipitation of gold in the form of spherical and irregular plate-like nanoparticles on the terraces of the support.

Therefore, the shape of gold nanoparticles rules the selectivity of these catalysts in the 5-hydroxymethylfurfural oxidative esterification reaction.

## 4. Conclusions

Zirconia supported catalysts are active in the HMF oxidative esterification even without the use of a base such as sodium methoxide which makes the process less sustainable from an environmental and economic point of view. The best catalytic activity was observed with gold supported on a sulphated zirconia with a low percentage of sulphate groups (2 wt% nominal sulphates content).

It has been observed that the amount of sulphates not only increases the surface area of zirconia and the gold amount and dispersion, but it also has an effect on the gold shape (according to the observed DRUV-Vis plasmonic absorptions and the HRTEM findings). A relationship between the shape of the gold active phase and the catalytic performances has been proposed. Indeed, the presence of irregular plate-like gold nanoparticles is suggested to affect the selectivity of the catalytic system.

## 5. Acknowledgments

We thank Mrs. Tania Fantinel for technical assistance. Financial support to this work by MIUR (Cofin 2008) is gratefully acknowledged.

## 6. References

[1] B. Kamm, P. Gruber, M. Kamm (2005) "Biorefineries—industrial processes and products, status quo and future directions", vols 1 and 2, Wiley-VCH, Weinheim.

[2] H. Röper, Starch 54 (2002) 89–99.

[3] S. Albonetti, T. Pasini, A. Lolli, M. Blosi, M. Piccinini, N. Dimitraos, J.A. Lopez-Sanchez, D.J. Morgan, A.F. Carley, G.J. Hutchings, F. Cavani, Catal. Today, 195 (2012) 120-126.

[4] Y.Y. Gorbanev, S.K. Klitgaard, J.M. Woodley, C.H. Christensen, A. Riisager, ChemSusChem 2 (2009) 672-675.

[5] X. Tong, Y. Ma, Y. Li, Appl. Catal. A 385 (2010) 1-13 and references therein.

[6] A. Gandini, A.J.D. Silvestre, C.P. Neto, A.F. Sousa, M. Gomes, J. Polym. Sci. Pol. Chem., 47 (2009) 295-298.

[7] R. J. Sheehan, in Ullmann's Encyclopedia of Industrial Chemistry, vol A26, VCH Verlags, Weinheim,1995, p.193.

[8] F. Menegazzo, T. Fantinel, M. Signoretto, F. Pinna, Catal. Commun. 8 (2007) 876-879.

[9] E. Taarning, I. S. Nielsen, K. Egeblad, R. Madsen, C. H. Christensen, ChemSusChem 1 (2008) 75-78.

[10] O. Casanova, S. Iborra, A. Corma, J. Catal. 265 (2009) 109-116.

[11] S. E. Davis, M. S. Ide, R. J. Davis, Green Chem. 15(2013) 17-45.

[12] X. Tong, Y. Ma, Y. Li, Appl. Catal. A, 385 (2010)1-13.

[13] A. Rosatella, S. P. Simeonov, R. F. M. Frade, C. A. M. Afonso, Green Chem. 13 (2011) 754-793.

[14] O. Casanova, S. Iborra, A. Corma, ChemSusChem, 2 (2009) 1138-1144.

[15] N.K. Gupta, S. Nishimura, A. Takagaki, K. Ebitani, Green Chem., 13 (2011) 824-827.

[16] J. Cai, H. Ma, J. Zhang, Q. Song, Z. Du, Y. Huang, J. Xu, Chem. Eur. J., 19 (2013) 14215-14223.

[17] F. Pinna, A. Olivo, V. Trevisan, F. Menegazzo, M. Signoretto, M. Manzoli, F. Boccuzzi, Catal. Today 203 (2013) 196-201.

[18] M. Signoretto, F. Menegazzo, L. Contessotto, F. Pinna, M. Manzoli, F. Boccuzzi, Appl. Catal. B. 129 (2013) 287- 293.

[19] M. Signoretto, F. Menegazzo, F. Pinna, M. Manzoli, V. Aina, G. Cerrato, F. Boccuzzi, J. Catal., 309 (2014) 241-247.
[20] F. Menegazzo, T. Fantinel, M. Signoretto, F. Pinna, M. Manzoli, J. Catal., 319 (2014) 61–70.
[21] M. Manzoli, F. Boccuzzi, V. Trevisan, F. Menegazzo, M. Signoretto, F. Pinna, Appl. Catal. B 96, (2010) 28-33.
[22] Sample number 17C, supplied by World Gold Council, http://www.gold.org.
[23] S.J. Gregg, K.S.W. Sing, Adsorption, Surface Area and Porosity – 2nd ed., Academic Press, 1982, p. 111.
[24] F. Menegazzo, F. Pinna, M. Signoretto, V. Trevisan, F. Boccuzzi, A. Chiorino, M. Manzoli, Appl. Catal., A. 356 (2009) 31-35.
[25] C. Morterra, G. Cerrato, M. Signoretto, Catal. Lett., 41 (1996) 101.
[26] M. Signoretto, F. Pinna, G. Strukul, P. Chies, G. Cerrato, S. Di Ciero, C. Morterra, Journal of Catalysis 167 (1997) 522–532.
[27] E. Kowalska, O.O. Prieto Mahaney, R. Abe, B. Ohtani, Phys. Chem. Chem. Phys., 2010, 12, 2344-2355.
[28] J. Tiggesbaumker, L. Koller, H.O. Lutz, K.H. Meiwesbroer, Chem. Phys. Lett., 190 (1992) 42.
[29] A. Leibsch, Phys. Rev. B: Condens. Matter, 48 (1993) 11317.
[30] A. Moores, F. Goettmann, New J. Chem., 30 (2006) 1121-1132.
[31] M. Maillard, S. Giorgio, M.-P. Pileni,J. Phys. Chem. B, 107 (2003) 2466-2470.
[32] T.K. Sau, C.J. Murphy, J. Am. Chem. Soc., 126 (2004) 8648-8649.
[33] M. Hu, J. Chen, Z.-Y. Li, L. Au, G.V. Hartland, X. Li, M. Marquez, Y. Xia, Chem. Soc. Rev., 35 (2006) 1084–1094.
[34] J. Zhu, L. Huang, J. Zhao, Y. Wang, Y. Zhao, L. Hao, Y. Lu, Mater. Sci. Eng. B, 121 (2005) 199.
[35] J.-E. Park, T. Momma, T. Osaka, Electrochim. Acta, 52 (2007) 5914.
[36] E. Hao, R.C. Bailey, G.C. Schatz, J.T. Hupp, S. Li, Nano Lett., 4 (2004) 327-330.

**Captions**

**Table 1:** Textural properties of the supports

**Table 2:** Characterization data obtained for the catalysts

**Table 3:** Optical properties of the catalysts

**Figure 1:** XRD patterns of bare zirconia (Z), 2 wt% (SZ2) and 8 wt% (SZ8) sulphated zirconia samples.

**Figure 2:** $N_2$ physisorption isotherms of Z (squares), SZ2 (triangles) and SZ8 (stars) supports and (insert) their BHJ pore size distributions.

**Figure 3:** XRD patterns of the Au catalysts (section a) and zoom on the 37-40 2θ range.

**Figure 4:** FTIR absorbance spectra of 2.5 mbar adsorbed CO at -116 °C.

**Figure 5:** Catalytic performances for the oxidative esterification of HMF to FDMC. (reaction at 130 °C - 3 bar $O_2$ - 5 h of reaction).

**Figure 6:** Diffuse Reflectance Spectra of the as prepared catalysts.

**Figure 7:** Image taken on the as prepared catalysts.

**Figure 8:** HRTEM images collected on AuSZ8: roundish Au nanoparticles (signaled by arrows in section a), irregular plate-like Au particle on $ZrO_2$ (section b), Au particle size distribution (section c). Instrumental magnification: 300000X and 800000X, respectively.

**Scheme 1**. Composition of lignocellulosic biomass.

**Scheme 2**. HMF oxidative esterification reaction.

**Scheme 3** Possible mechanism of the effect of sulphates on gold active phase: a) different amounts of sulphated groups on zirconia; b) calcination at 650 °C; c) deposition-precipitation of gold (represented by violet spheres).

**Scheme 4:** Possible effect of sulphates on the shape of gold species: deposition-precipitation of gold in the form of spherical and irregular plate-like nanoparticles on the terraces of the support.

**Table 1:** Textural properties of the supports

| | Nominal $SO_4^=$ (%) | Found $SO_4^=$ (%) | Surface area ($m^2/g$) | Mean pore size (nm) |
|---|---|---|---|---|
| Z | 0 | 0 | 84 | 12.6 |
| SZ2 | 2 | 1.4 | 122 | 9.0 |
| SZ8 | 8 | 3.4 | 129 | 8.4 |

**Table 2:** Characterization data obtained for the catalysts

| | Effective Au content (%) | Surface area ($m^2/g$) | Mean pore size (nm) | Chemisorption ($mol_{CO}/mol_{Au}$) |
|---|---|---|---|---|
| AuZ | 1.1 | 84 | 12.6 | 0.042 |
| AuSZ2 | 1.2 | 122 | 9.0 | 0.045 |
| AuSZ8 | 1.3 | 129 | 8.4 | 0.052 |
| AuWGC | 1.5 | 55 | 29.0 | 0.033 |

**Table 3:** Optical properties of the catalysts

| | Color | LSPR (nm) |
|---|---|---|
| AuWGC | violet | 545 |
| AuZ | purple | 540 |
| AuSZ2 | dark purple-violet | 522 and 597 |
| AuSZ8 | dark violet-grey | 525 and 624 |

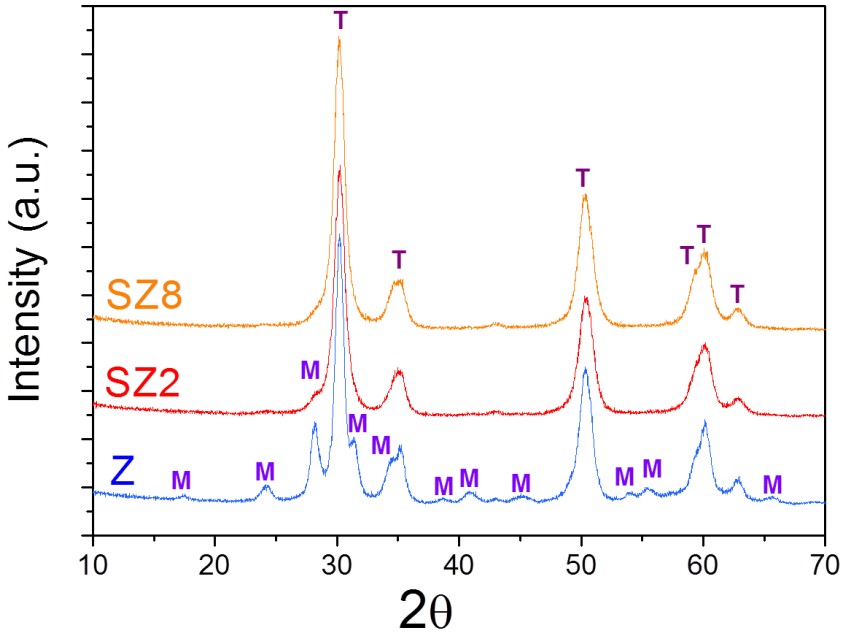


**Figure 1:** XRD patterns of bare zirconia (Z), 2 wt% (SZ2) and 8 wt% (SZ8) sulphated zirconia samples.

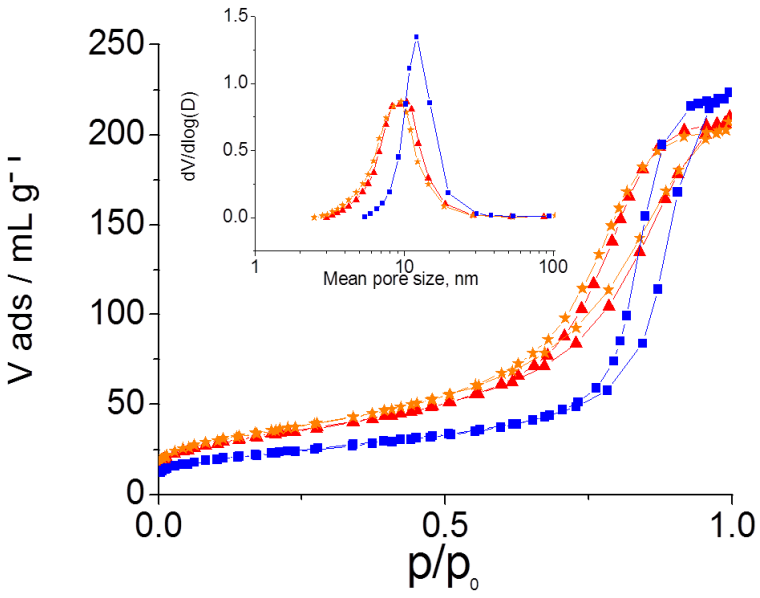


**Figure 2:** $N_2$ physisorption isotherms of Z (squares), SZ2 (triangles) and SZ8 (stars) supports and (insert) their BHJ pore size distributions.

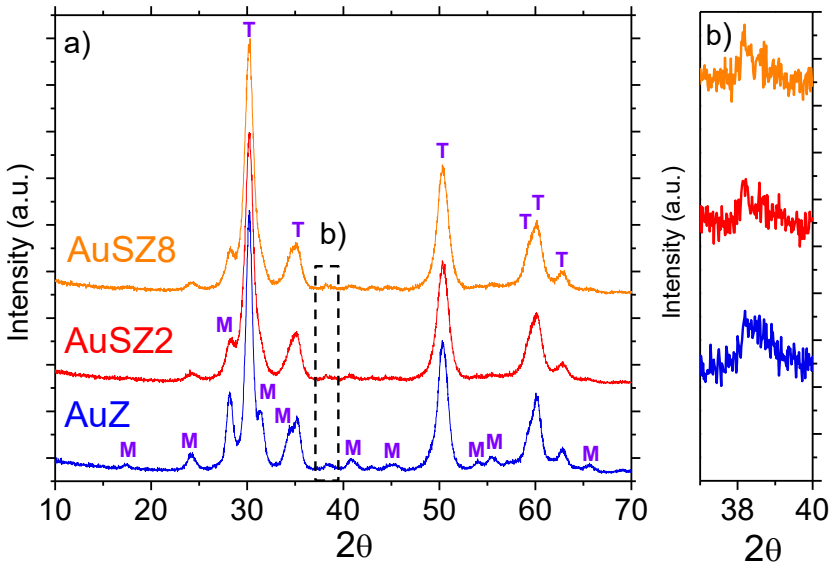


**Figure 3:** XRD patterns of the Au catalysts (section a) and zoom on the 37-40 2θ range.

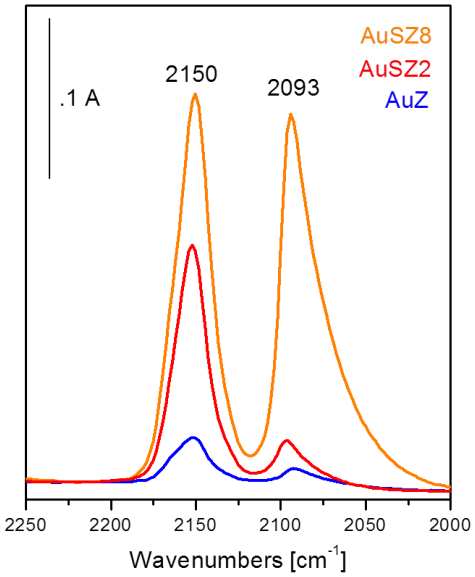


**Figure 4:** FTIR absorbance spectra of 2.5 mbar adsorbed CO at -116 °C.

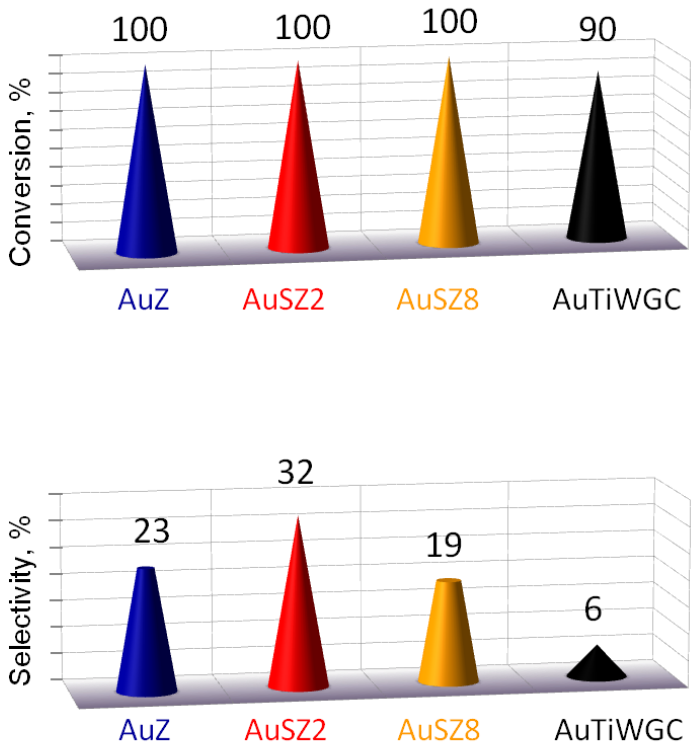


**Figure 5:** Catalytic performances for the oxidative esterification of HMF to FDMC. (reaction at 130 °C - 3 bar $O_2$ - 5 h of reaction).

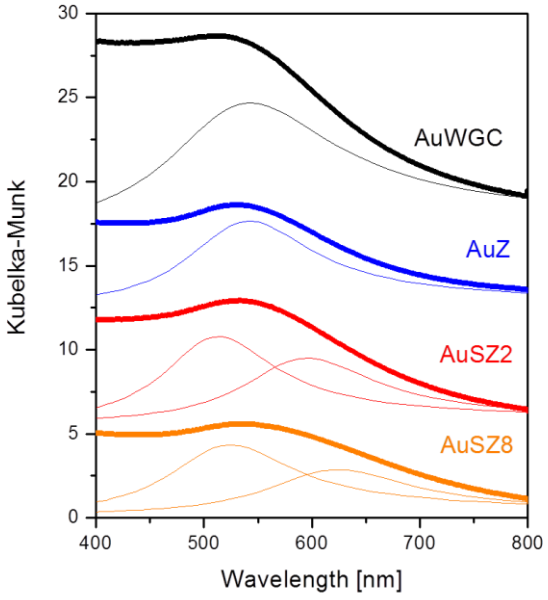


**Figure 6:** Diffuse Reflectance Spectra of the as prepared catalysts.

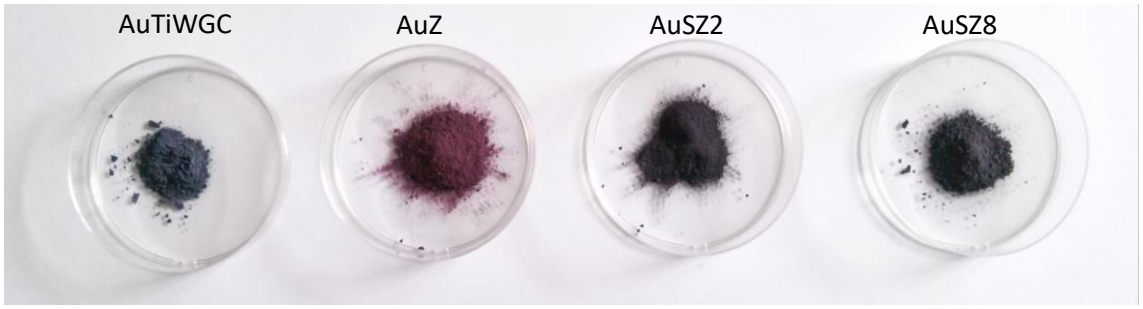


**Figure 7:** Image taken on the as prepared catalysts.

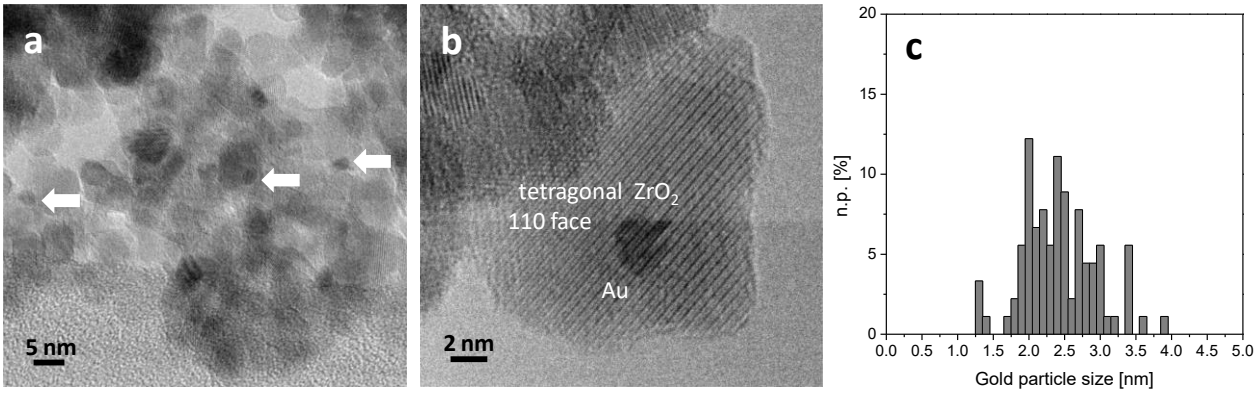


**Figure 8:** HRTEM images collected on AuSZ8: roundish Au nanoparticles (signaled by arrows in section a), irregular plate-like Au particle on $ZrO_2$ (section b), Au particle size distribution (section c). Instrumental magnification: 300000X and 800000X, respectively.